Accepted Manuscript

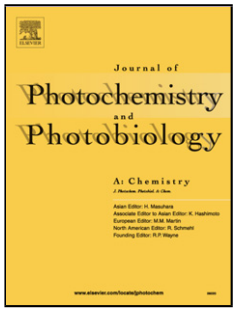

Title: New pyrazolo-quinoline scaffold as a reversible colorimetric fluorescent probe for selective detection of Zn^{2+} ions and its imaging in live cells

Authors: Kasirajan Gayathri, Krishnaswamy Velmurugan, Raju Nandhakumar, Mahalingam Malathi, Sadasivam Mathusalini, Palathurai Subramaniam Mohan, Ramasamy Shankar

PII: S1010-6030(17)30126-0
DOI: http://dx.doi.org/doi:10.1016/j.jphotochem.2017.03.035
Reference: JPC 10586

To appear in: *Journal of Photochemistry and Photobiology A: Chemistry*

Received date: 28-1-2017
Revised date: 25-3-2017
Accepted date: 26-3-2017

Please cite this article as: Gayathri Kasirajan, Velmurugan Krishnaswamy, Raju Nandhakumar, Malathi Mahalingam, Mathusalini Sadasivam, Mohan Palathurai Subramaniam, Shankar Ramasamy, New pyrazolo-quinoline scaffold as a reversible colorimetric fluorescent probe for selective detection of Zn2+ ions and its imaging in live cells, Journal of Photochemistry and Photobiology A: Chemistryhttp://dx.doi.org/10.1016/j.jphotochem.2017.03.035

New pyrazolo-quinoline scaffold as a reversible colorimetric fluorescent probe for selective detection of Zn^{2+} ions and its imaging in live cells

Kasirajan Gayathri [a], Krishnaswamy Velmurugan [b], Raju Nandhakumar [b*], Mahalingam Malathi [c], Sadasivam Mathusalini [a], Palathurai Subramaniam Mohan [a*], Ramasamy Shankar [d]

[a] *Department of Chemistry, Bharathiar University, Coimbatore 641 046, Tamil Nadu, India.*
[b] *Department of Chemistry, Karunya University, Coimbatore 641 114, Tamil Nadu, India.*
[c] *Department of Chemistry, Bannari Amman Institute of Technology, Sathyamangalam 638 401, Tamil Nadu, India*
[d] *Department of Physics, Bharathiar University, Coimbatore 641 046, Tamil Nadu, India.*

**Corresponding author. Tel.: +919363211210*
E-mail address: ps_mohan_in@yahoo.com, psmohan59@gmail.com (P.S. Mohan).
nandhakumar@karunya.edu (R. Nandhakumar).

Graphical abstract

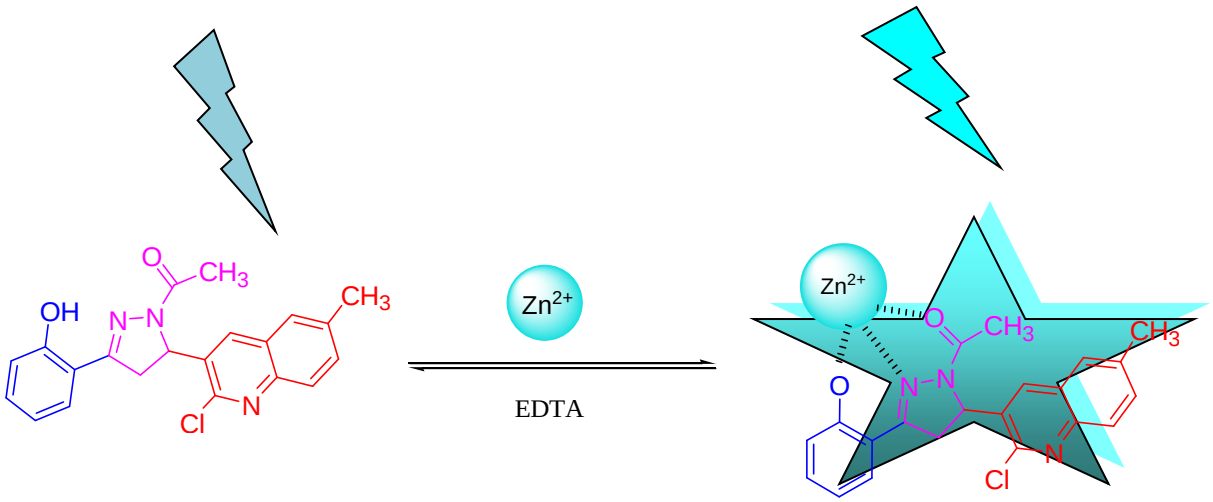

Highlights

- Pyrazoline based chemosensor was synthesized that selectively detects zinc ion.
- Naked eye color change from colorless to yellow is due to OFF-ON process, photoinduced electron transfer (PET) and CHEF.
- The limit of detection (LOD) of probe with Zn^{2+} ion is 2.9 nM.
- Density functional theory calculations further supports the fluorescence change.
- The sensitivity of probe is demonstrated successfully for selective imaging of Zn^{2+} in living cells.

Abstract

A simple colorimetric fluorescent chemosensor 1-[5-(2-chloro-6-methylquinolin-3-yl)-3-(2-hydroxyphenyl)-4,5-dihydro-*1H*-pyrazol-1-yl]ethan-1-one (**L**) based on pyrazoline has been designed, synthesized and characterized. The sensing properties of **L** were studied using UV–Visible and fluorescence spectrophotometric analyses. **L** showed excellent selectivity towards Zn^{2+} ions over other metal ions in aqueous media through "OFF-ON" type process and a possible photoinduced electron transfer (PET). The viability of **L** to Zn^{2+} has been demonstrated by live cell imaging.

Keywords

Quinoline; Chemosensor; Zinc; Colorimetric; Fluorimetric; Bioimaging

1. Introduction

In recent years, development of chemosensors witnessed remarkable progress in the detection of transition and heavy metal ions and it has widespread applications in the field of analytical chemistry, biology and environmental processes[1-10]. Chemosensors based on cation induced fluorescence changes have advantage of possessing high sensitivity, selectivity,

simplicity and instantaneous response [8, 11-13]. Neurobiological processes relevant to human health and diseases are primarily controlled by Zinc ions. Zn^{2+} is the second most abundant and essential element after Fe^{2+} and Fe^{3+} ions in human and performs a variety of functions. The decrease in concentration of Zn^{2+} in human body causes diseases such as Alzheimer's disease, β-thalassemia, Parkinson's disease, ischemic stroke and epilepsy[14-19]. Zinc decreases copper burden and has been used effectively to treat Wilson's disease and also in the treatment of hepatic encephalopathy, sickle cell disease, diabetes and malignancy. The cell culture studies showed that zinc activates nuclear factor kappa B in T helper cells and deficiency of it reduces the binding of nuclear factor kappa B to deoxyribonucleic acid, leading to decreased gene expression of interleukin 2 and its production[20, 21]. Hence, there is a need for the development of artificial chemosensors for recognition of Zn^{2+} ions in environmental as well as biological samples. However, selective recognition of zinc in the presence of other cations is a tedious task as closed shell d^{10} electronic configuration totally affects the redox and spectral features.

Recently, fluorescent sensors for zinc ions have made their mark in the field of molecular recognition. Several zinc sensors have been developed based on different fluorophores such as quinoline, fluorescein, coumarin, peptide, pyrene and proteins with apparent dissociation constants in the micro to nano molar ranges[22-32]. Particularly, more attention has been paid to quinoline fluorophore due to its strong binding ability with metal ions, altering the molecular size based on coordinating systems and high quantum yield which plays a vital role to detect metal ions in biological and living systems[33, 34]. Nevertheless, only a few researchers have reported on detection of Zn^{2+} ion through dual pathways such as colorimetric and fluorescent turn 'off-on' signaling system[35-39]. In this connection, there are number of issues to be addressed while devising suitable zinc sensors such as selectivity, binding ratio, suitability in live cells. Therefore, designing a suitable sensor capable of detecting Zn^{2+} ions *via* colorimetric and fluorescent sensing methods is desirable in the field of environmental and biological sciences. Hence our efforts were directed to the preparation of suitable sensor by following a simple route and easily accessible chemicals.

Herein, we report a quinoline-pyrazoline chemosensor (**L**), that selectively detect Zn^{2+} ion, using colorimetric and fluorescent techniques. This sensor **L** is designed in such a way that quinoline acts as a fluorophore, which is covalently attached to a pyrazoline and hydroxy phenyl

rings through a C-C spacer unit. The hetero atoms of pyrazoline ring containing 'N', acetyl 'O' and hydroxy phenyl 'O' act as binding sites to recognize Zn^{2+} ion. This is the first example of quinoline-pyrazoline based sensor **L** for selective detection of Zn^{2+} ion by colorimetric and fluorimetric methods.

2. Experimental

2.1. Reagents and instruments

All reagents were of analytical grade and doubly distilled water was used throughout the analysis. 2'-hydroxyacetophenone was obtained from Sigma Aldrich. Other reagents were purchased from commercial suppliers and used without further purification. ^{1}H NMR and ^{13}C NMR spectra were recorded on a Bruker 400 MHz and 100MHz spectrometer and DMSO solution with tetramethyl silane (TMS) as internal standard. LC–MS was recorded on a LC–MSD-Trap-XCT Plus based on infusion methods. A Nicolet Avatar Model FT-IR spectrophotometer was used to record IR spectra (4000–400 cm^{-1}). Microanalyses were examined on a Vario EL III model CHNS/O analyzer (Vario, Germany) and Scanning Electron microscope (SEM) studies were performed on JEOL model JSM- 6390. UV–visible absorption spectra were measured using JASCO-V- 630 spectrophotometer. Fluorescence measurements were performed on JASCO FP-6600 spectrofluorometer equipped with quartz cuvettes of 1 cm path length. The excitation and emission slit width were 5.0 nm. All emission spectra were recorded at 24 ± 1 °C. Stock solutions for analysis were prepared (2 $\times 10^{-6}$ M for compound **L** ($EtOH/H_2O$, 1:1 (v/v), HEPES = 50 mM, pH = 7.2) immediately before the experiments. The solutions of metal ions were prepared from nitrate salts of Na^{+}, K^{+}, Al^{3+}, Cu^{2+}, Cd^{2+}, Hg^{2+}, Pb^{2+}, Zn^{2+}, Co^{2+}, Ni^{2+}, Ca^{2+}, Mn^{2+}, Cr^{3+}, Ba^{2+}, Mg^{2+}, Fe^{2+}, Fe^{3+}, Zr^{2+}, Ce^{3+} and Ag^{+}.

2.2. Synthesis of 1-[5-(2-chloro-6-methylquinolin-3-yl)-3-(2-hydroxyphenyl)-4,5-dihydro-1H-pyrazol-1-yl]ethan-1-one (L)

Chalcone **3** was easily prepared from compound **1** and **2** in 79 % yield, according to the literature[40]. An equimolar mixture of compound **3** (3.2 g, 0.01 mol) and hydrazine hydrate (0.5

g, 0.01 mol) were taken in a 100 ml reaction flask in the presence of glacial acetic acid (15 ml) and refluxed at 120° C for 6 h. After completion of reaction, it was cooled and poured into crushed ice. The resulting precipitate was filtered and recrystallized from ethyl acetate to yield probe **L**. Pale yellow solid; Mp. 232 ºC; Yield: 74.33 %; FT-IR (KBr): 3430 (-OH), 1664 (C=O) and 1101 cm^{-1} (C-N). ^{1}H NMR (DMSO-*d6*, 400 MHz) δ ppm: δ 10.18 (s, 1H, OH), 8.03 (s, 1H, Ar-H), 7.81-7.85(m, 2H, Ar-H), 7.63(d, 1H, *J* = 8.4 Hz, Ar-H), 7.56(d, 1H, *J* = 8 Hz, Ar-H), 7.32(t, 1H, *J* = 6.8 Hz, Ar-H), 6.88-6.97(m, 2H, Ar-H), 5.79 (dd, 1H, *J* = 12 Hz, *J* = 5.2 Hz, CH in pyrazoline moiety), 4.07-4.14 (m, 2H, CH_2 in pyrazoline moiety), 2.48(s, 3H, $COCH_3$), 2.38(s, 3H, CH_3); ^{13}C NMR (DMSO-*d6*, 100 MHz) δ ppm: 178.07, 160.93, 152.10, 143.68, 137.14, 135.69, 135.02, 128.33, 127.83, 126.10, 125.52, 125.34, 124.77, 124.12, 123.67, 122.09, 109.90, 34.45, 31.15, 25.35, 17.83; LCMS (ESI^+) *m/z* Calculated: 379.11, Found: 378.2 [$(M-1)^+$]; Calculated For $C_{21}H_{18}N_3O_2Cl$ (379.11): C, 66.40; H, 4.78; N, 11.06, Found: C, 67.54; H, 4.90; N, 11.49 %.

2.3. Theoretical studies

Both probe **L** and **L**-Zn^{2+} were optimized using density functional theory (DFT) by employing B3LYP[41] functional and LANL2DZ[42-44] basis set. The optical absorption and emission spectra for **L** and **L**-Zn^{2+} were calculated using time dependent density functional theory (TDDFT). All structures were optimized in ethanol medium using PCM model[45]. To calculate emission spectra, the structures were optimized in excited state using TD-B3LYP/LANL2DZ basis set. The frequency calculations were done for **L** and **L**-Zn^{2+} in order to ensure optimized ground state and the computation was carried out using G09 software program[46].

2.4. Cytotoxicity study by MTT (3-(4,5-dimethylthiazol-2-yl)-2,5-diphenyltetrazolium bromide) assay and fluorescence imaging

A cytotoxicity of probe **L** was carried out on mouse neuroblastoma (N2A) cancer cell lines which were obtained from National Center for Cell Science (NCCS), Pune, India. Cell

viability was carried out using the MTT assay method[47]. Cells were maintained in minimum essential Eagle's medium (Sigma Aldrich, India) supplemented with 10 % fetal bovine serum (FBS), streptomycin (100 µg/ml), penicillin (100 U/ ml) and essential amino acids (Himedia, India). The cells were plated at a density of 7×10^3 in 96-well cell cultured plate and incubated in a humidified chamber with 95 % air, 5 % CO_2 and 100 % relative humidity for 24 h prior to the addition of compound. The probe **L** was dissolved in dimethyl sulphoxide (DMSO) and diluted in the respective medium with 1% FBS containing the probe at various concentrations and incubated at 37 ºC with 95 % air, 5 % CO_2 and 100 % relative humidity for 48 h. After 48 h, 10 µL of MTT (5 mg/mL) in phosphate buffered saline (PBS) was added to each well and incubated for 4 h at 37 ºC. The medium with MTT was then flicked off and as a result formazan crystals were dissolved in 100 µL of DMSO. The absorbance was then measured at 570 nm using a microquant plate reader (Bio-Tek Instruments).

For bioimaging, cells were seeded at a density of 2×10^4 in 24-well cell culture plate and allowed to settle for 12 h. When cells attained 80 % confluence, the media was changed. Cells were treated with **L** (10 µM) alone for 3 h and then treated with Zn^{2+} (10 µM) and the plate was incubated for 3 h in a humidified incubator at 37 ºC with 95 % air and 5 % CO_2. The fluorescence of probe **L** localized was captured under inverted fluorescence microscope (EVOS, Life Technologies, USA).

2.5. Scanning Electron Microscope (SEM) studies

The probe **L** and **L**+Zn^{2+} were dissolved in small amount of acetone. By using drop-casting method, the samples were coated over silicon bare wafer and placed in the hot air oven at 60 °C for 5 hours to get thin film samples. Then before taking SEM images Pt was coated by sputtering to avoid charging effect. The film uniformity is evenly agglomerated which can be seen in lower magnification of SEM images.

3. Results and Discussion

The fluorescent probe **L** was conveniently synthesized from 2-chloro-6-methylquinoline-3-carbaldehyde[48] by two steps, as shown in Scheme 1. The reaction between quinoline

carbaldehyde (**1**) and 2'-hydroxyacetophenone (**2**) in ethanol afforded compound **3** by Claisen-Schmidt type of condensation process. Subsequently, **3** and hydrazine hydrate were reacted in the presence of glacial acetic acid under reflux condition to obtain **L** in reasonable yield through addition and cyclization process. The structure of **L** was confirmed by standard spectroscopic and analytical techniques such as NMR (^{1}H and ^{13}C) and mass spectrometry (Fig. S1-S3).

Scheme 1.

The selective detection of probe **L** was done by using UV- visible absorption spectrum in EtOH-H_2O (1:1 v/v, HEPES= 50 mM, pH=7.2) solution. The spectrum showed two intense absorption bands centered at 280 and 323 nm (Fig. 1). Upon addition of Zn^{2+} ion (50 equiv) to **L**, considerable changes in the two absorption bands occurred followed by a new shoulder band appearing at 380 nm. Also, a significant color change from colorless to pale yellow was observed by naked eye which is due to d-d transition between metal to ligand charge transfer (MLCT) complex. Addition of other metal ions such as Na^{+}, K^{+}, Cu^{2+}, Cd^{2+}, Ni^{2+}, Hg^{2+}, Pb^{2+}, Co^{2+}, Ca^{2+}, Mn^{2+}, Cr^{3+}, Ba^{2+}, Mg^{2+}, Fe^{2+}, Fe^{3+}, Al^{3+}, Zr^{2+}, Ce^{3+} and Ag^{+} to **L** did not show any spectral and color changes. The results reveal that probe **L** coordinate well with Zn^{2+} ion in EtOH-H_2O (1:1 v/v, HEPES= 50 mM, pH=7.2) solution, with an apparent color change. Furthermore, the sensing behavior of **L** was examined with Zn^{2+} based different counter ions such as $ZnSO_4$, $Zn(NO_3)_2$, $ZnCl_2$, $Zn(CH_3COO)_2$ as shown in supporting information (Fig. S11). L bind with different salts of Zn^{2+} and the emission intensity were found to be almost similar in all the cases. These observations show that the counter ions do not play an important role in the selectivity of Zn^{2+} using L. This indicates that probe L shows selective emission enhancement towards Zn^{2+}.

Fig. 1.

In continuation of the above findings, UV-Vis titration experiments were carried out by consecutive addition of Zn^{2+} ions (0 to 25 equiv.) to **L**. The absorbance bands at 280 and 323 nm of **L** steadily decreases with an increase in the concentration of Zn^{2+} ions. Simultaneously, an

isosbestic point and a shoulder peak were observed at 358 and 380 nm respectively (Fig. 2), which indicates the formation of a coordination complex between **L**–Zn^{2+}. Thus, probe **L** acts as a ratiometric and naked eye sensor for Zn^{2+} ions *via* colorimetric method.

Fig. 2.

Metal ion binding ability of **L** was carried out with various transition metal ions by using fluorescence spectrometric technique (Fig. 3). The emission spectra of **L** showed a weak band at 408 nm with quantum yield. Upon addition of Zn^{2+} ions to solution **L**, a small red shift with fluorescence enhancement was observed. The change in spectral wavelength from 408 to 418 nm is due to an inhibition of photo-induced electron transfer (PET) process and restricted C=N isomerization mechanism[49, 50]. This 10 nm red shift is clearly shown in the normalized spectrum (Fig. S4). Under identical conditions, addition of other metal ions (Na^{+}, K^{+}, Cu^{2+}, Cd^{2+}, Ni^{2+}, Hg^{2+}, Pb^{2+}, Co^{2+}, Ca^{2+}, Mn^{2+}, Cr^{3+}, Ba^{2+}, Mg^{2+}, Fe^{2+}, Fe^{3+}, Al^{3+}, Zr^{2+}, Ce^{3+} and Ag^{+}) to **L**, did not show any significant changes in the emission profiles. Thus, probe **L** can selectively senses Zn^{2+} ions by fluorescence "turn off-on" process.

Fig. 3.

The effect of pH on probe **L** and **L**-Zn^{2+} with different pH values were recorded by fluorescence spectra. The experiments revealed that **L** showed a weak fluorescence intensity between pH 0 and 14, whereas in the presence of Zn^{2+}, fluorescence intensity of **L** increased dramatically between pH 5 and 8 and reached the maximum at pH 7 (Fig S5). Therefore, we have chosen physiological pH for all biological studies like live cell imaging.

The time-dependent fluorescence intensity changes of **L** with Zn^{2+} was studied and results are shown in Fig S6. It showed that **L** completely coordinates with Zn^{2+} in almost 5 min and after that no noticeable changes was observed. Therefore, we have selected the incubation time of 15 minutes for all spectral studies.

To find the practical applicability of **L**, interference studies were carried out in the presence of 50 equiv. of Zn^{2+}, treated with same equiv. of other potential metal ions is shown in

Fig. 4. No obvious interference in emission spectrum was found on comparison with other competitive metal ions besides Zn^{2+}. In general, most of the Zn^{2+} sensors found Cd^{2+} ion interferences due to same periodic behavior with Zn^{2+}. Surprisingly, **L**-Zn^{2+} complex eliminated the influence of Cd^{2+} ion by blocking PET, CHEF and restricted C=N isomerization mechanism. These results establishes that **L** strongly coordinates with Zn^{2+} ion which could be used to distinguish Zn^{2+} from Cd^{2+} ion in real applications.

Fig. 4.

To evaluate the chemosensing behavior of **L**, fluorescence titration experiments were carried with various concentrations of Zn^{2+} ions. Upon gradual addition of Zn^{2+} from 0 to 25 equiv., the fluorescence intensity of **L** at 408 nm steadily increased with a small red shift. The fluorescence changes of L upon addition of Zn^{2+} is shown in Fig. 5.

Fig. 5.

The quantum yield φ[51] was calculated by using the following equation,

$$\varphi x = \varphi s(F_x/F_s)(A_s/A_x)(\eta^2_x/\eta^2_s).$$

where, x and s indicate the unknown and standard samples, φ-quantum yield, F is the integrated fluorescence intensity, A-absorbance, and η- refractive index of the solvent.(Quinine sulphate [52] as standard in 0.1 M H_2SO_4[φ=0.54]). The quantum yield of **L** is 0.019, and on complexation with Zn^{2+}, the value significantly increased to 0.214. The binding ratio of **L**-Zn^{2+} (Host-Guest) complex was investigated by Job's plot continuous variation methods [53] is shown in Fig. 6. The maximum mole fraction of **L** was appeared at 0.5, which supported a 1:1 (**L**: Zn^{2+}) binding stoichiometry. It was further advocated by Benesi–Hildebrand nonlinear curve fitting method [54, 55](Fig. 7). The binding constant of **L**-Zn^{2+} complex was found to be $Ka = 1.88 \times 10^4\ M^{-1}$ and the limit of detection (LOD) of probe **L** is 2.9 nM, calculated using 3δ/S [56]. The high sensitivity and low detection limit of **L** could be used as a trace level identification of Zn^{2+} in real level environmental samples. Moreover, Zn^{2+} ion concentration in human body ranges from 3 nM to 10 μM and can be monitored by this probe **L** [57, 58]. The

advantage of preparing the above compound and its detection limit is realized when compared with other zinc sensors reported in the literature with their corresponding detection limit **(Table 1).**

Fig. 6.

Fig. 7.

Table 1.

The interaction of the probe **L** with Zn^{2+} was investigated through ^{1}H NMR spectroscopy. This experiment was performed to further support the coordination structure for Zn^{2+} complex with **L** in DMSO-d_6. Fig. 8 shows the ^{1}H NMR spectra of L with and without Zn^{2+}. All the chemical shifts were identified by the ^{1}H NMR titration analysis. During the addition of Zn^{2+} to probe **L** and upon increasing the concentration of Zn^{2+} ions gradually (0.5, 1.0, 1.5 and 2.0 equiv.) the hydroxyl peak at 10.15 ppm decreases and almost disappeared on addition of 2.0 equiv. of Zn^{2+}. In addition, small upfield shifts were noticed in the aromatic region and for the methyl and the methoxy protons. These shifts clearly advocates the complex formation between the probe L and Zn^{2+} wherein the hydroxyl and C=N groups are involved in the coordination.

Fig. 8.

As shown in Fig. 9, FT-IR spectrum of **L**, showed characteristic bands at 3430 cm^{-1}, 1664 cm^{-1} and 1101 cm^{-1} assigned to -OH, pyrazoline C=O and C-N stretching respectively [59-63]. On addition of Zn^{2+} to **L**, two bands shifted downward from 3430 and 1664 cm^{-1} to 3314 and 1632 cm^{-1} respectively and C-N stretching band at 1101 cm^{-1} shifted to 1112 cm^{-1}, which is due to decrease in electron density *via* the coordination of –OH, C=O and C=N groups with Zn^{2+} (see Scheme 2).

Fig. 9.

Furthermore, in order to understand the morphological differences, the Scanning Electron Microscope (SEM) images of probe **L** and **L**-Zn^{2+} was captured as shown in Fig. 10. The chemosensor **L** shows a random fibre network structure with microholes. However, upon probe **L** on complexation with Zn^{2+} ions, the fibre network structure with microholes were completely covered and agglomerated. The chemical composition of the **L**- Zn^{2+} complex is measured by the EDX analysis (Fig. 10 and Table S1) which clearly showed the presence of carbon (C), oxygen (O), chlorine (Cl) and Zn elements in the prepared **L**- Zn^{2+} Complex.

Fig. 10.

The recognition reversibility of **L** was further verified with EDTA by fluorescence experiments. The addition of Zn^{2+} (50 equiv.) to probe **L** showed remarkable enhancement in its fluorescence intensity. Upon addition of EDTA (50 equiv.) to **L**-Zn^{2+} solution, emission intensity get quenched and almost reached the intensity of original receptor **L** due to EDTA-Zn^{2+} complex formation. This indicates, Zn^{2+} recognition process is reversible (Fig. 11).

Fig. 11.

In order to evaluate absorption and emission behaviors of probe **L** and **L**-Zn^{2+} complex, we have performed quantum chemical TDDFT calculations using Gaussian 09 program. The optimized geometries and TD spectra of **L** and **L**-Zn^{2+} complex are shown in supporting information (Fig. S7 and S8). For probe L, absorption peak at 311 nm with oscillator strength 0.523 a.u was generated from HOMO to LUMO+1. While in the case of **L**-Zn^{2+} complex, transitions from HOMO-2 to LUMO and HOMO-1 to LUMO had contributed absorption values at 344 nm and 370 nm respectively. In computed spectrum, **L** showed emission at 342 nm and for **L**-Zn^{2+} complex, it was around 363 nm with oscillator strength 0.280 a.u. The difference from experimental wavelength is due to the basis set[64] used. The calculated absorption and emission spectra, orbital transition, wave length and its oscillator strength, are shown in supporting information (Table S2). Binding of Zn^{2+} leads to the lowering of energy gap of **L** from 3.982 eV (HOMO-LUMO+1) to 1.908 eV (HOMO-LUMO+4), 3.346 eV (HOMO-1 -

LUMO) and 3.595 eV (HOMO-2-LUMO). This might be the cause for formation of absorption bands at 344 nm and 370 nm[65].

Fig. 12.

For probe L, bond distances of N_1-N_2, N_2-C_{10}, C_{10}-C_{11}, C_{10}-O_2 and C_4-O_1 were calculated as 1.420 Å, 1.386 Å, 1.522 Å, 1.262 Å and 1.392 Å respectively. After complexation with Zn^{2+}, the donor sites were strained and changes in bond lengths were observed as 1.411 Å, 1.362 Å, 1.500 Å, 1.292 Å and 1.422 Å respectively. Further the coordination bond lengths of nitrogen atom of pyrazolyl and oxygen atoms of pyrazolyl and phenyl rings were found to be 2.085 Å, 2.076 Å and 2.106 Å respectively (Fig. S7). Hence it is clearly evident that, in probe **L**, HOMO is highly localized in the phenyl ring and a considerable amount of electron distribution is present in pyrazoline ring while LUMO is distributed around the quinoline ring (Fig. 12). After binding of Zn^{2+}, HOMO is distributed around quinoline ring and LUMO is resided around phenyl and pyrazoline rings. In LUMO+2, the electrons are centered on Zn^{2+} and in the case of HOMO-2, it spread over the entire molecule and this could be the cause for fluorescence enhancement of **L** upon addition of Zn^{2+}. The plots of frontier molecular orbitals of **L** and **L**-Zn^{2+} are shown in Figs S9 and S10.

Based on the results obtained, a plausible sensing mode for detection of Zn^{2+} by **L** is shown in Scheme 2. Probe **L** exhibited weak fluorescence intensity and addition of Zn^{2+} to **L**, leads to fluorescence enhancement and turn-on response with a red shift. This enhancement might be due to the combination of photo-induced electron transfer (PET) process and chelation-enhanced fluorescence (CHEF)[66] and the chelation of **L** with Zn^{2+} made the complex more rigid, which totally restrict C=N isomerisation[67, 68]. The 1:1 binding stoichiometry of **L**-Zn^{2+} complex was confirmed by titration studies, Job's plot and Benesi-Hildebrand nonlinear square curve fitting methods. Above results reveals that Zn^{2+} ion coordinates with C=N, C=O, -OH groups in 1:1 binding mode.

Scheme. 2.

The potential of receptor **L** was studied as 'ready to use indicator strips'. The experiments were done by using filter paper test strips dipped in solution of receptor **L** and **L**-Zn^{2+}. Both the strips were kept under exposure to UV light, the color of **L**-Zn^{2+} paper is changed to bright blue (Fig.13). Thus, **L** could be used as 'ready to use indicator strips' for detecting Zn^{2+} ions in EtOH-H_2O mixture (1:1 v/v, HEPES= 50 mM, pH=7.2).

Fig. 13.

To determine the practical applicability in biological systems, probe **L** was initially tested for bioimaging studies in N2A cell lines (Neuroblastoma cell lines from mouse). For this the cell viability was assessed by MTT assay *in vitro*. Three independent triplicates were done to determine the sensitivity of the probe **L** and the medium not containing the probe was served as the control. The percentage of cell inhibition was determined using the formula

% of inhibition = [mean OD of untreated cells (control) / mean OD of treated cells] × 100 and a graph was plotted as the percentage of cell inhibition versus concentration and from this the corresponding IC_{50} (the concentration that causes a 50% reduction of the cell growth) value was calculated as 37.10 ± 2.86 µM (Fig. 14). The concentration of probe **L** required for live cell imaging was determined by MTT assay and it was decided as 10 µM, which was less than IC_{50} value (37.10 ± 2.86 µM).

Fig. 14.

The fluorescence images recorded in green and red channels are shown in Fig. 15. The N2A cells incubated with probe **L** alone for 3 h displayed a weak intracellular fluorescence. Surprisingly, an enhanced intracellular fluorescence was observed in cells containing **L** incubated with Zn^{2+} for 3 h. From fluorescence and bright field measurements, it is confirmed that cells were sustainable throughout the imaging experiments. This reveals that probe **L** shows good cell permeability and also used to detect Zn^{2+} ions in living cells.

Fig. 15.

Conclusion

We have designed and synthesized a new reversible colorimetric fluorescent probe **L**, pyrazolo-quinoline conjugate, which showed enhanced fluorescence intensity in the presence of Zn^{2+} ions over other potentially competing metal ions in aqueous media. Thus **L** exhibits its advantage of using as a colorimetric, ratiometric and naked eye zinc sensor based on PET and CHEF mechanism. The binding constant of **L**-Zn^{2+} complex was found to be $K_a = 1.88\times 10^4\ M^{-1}$ and the limit of detection (LOD) of probe **L** with Zn^{2+} ions is 2.9 nM. The binding mode of probe **L** with Zn^{2+} was supported by DFT and TDDFT studies. Further, **L** has been used for live cell imaging of Zn^{2+} ions in N2A cells under physiological conditions.

Acknowledgement

P.S.M thanks, DRDO-BU-CLS (DLS/86/50071/DRDO-BU center /Phase-II) for providing financial support and instrument facility.

References

[1] M. Vonlanthen, N.S. Finney, Thioureas as Reporting Elements for Metal-Responsive Fluorescent Chemosensors, The Journal of Organic Chemistry, 78 (2013) 3980-3988.
[2] D.W. Domaille, E.L. Que, C.J. Chang, Synthetic fluorescent sensors for studying the cell biology of metals, Nat Chem Biol, 4 (2008) 168-175.
[3] A. Bencini, V. Lippolis, Probing biologically and environmentally important metal ions with fluorescent chemosensors: Thermodynamic versus optical response selectivity in some study cases, Coordination Chemistry Reviews, 256 (2012) 149-169.
[4] M. Formica, V. Fusi, L. Giorgi, M. Micheloni, New fluorescent chemosensors for metal ions in solution, Coordination Chemistry Reviews, 256 (2012) 170-192.
[5] R. McRae, P. Bagchi, S. Sumalekshmy, C.J. Fahrni, In Situ Imaging of Metals in Cells and Tissues, Chemical Reviews, 109 (2009) 4780-4827.
[6] H. Hisamoto, H. Tohma, T. Yamada, K.-i. Yamauchi, D. Siswanta, N. Yoshioka, K. Suzuki, Molecular design, characterization, and application of multi-information dyes for multi-

dimensional optical chemical sensing. Molecular design concepts of the dyes and their fundamental spectral characteristics, Analytica Chimica Acta, 373 (1998) 271-289.
[7] H.N. Kim, W.X. Ren, J.S. Kim, J. Yoon, Fluorescent and colorimetric sensors for detection of lead, cadmium, and mercury ions, Chemical Society Reviews, 41 (2012) 3210-3244.
[8] A.P. de Silva, H.Q.N. Gunaratne, T. Gunnlaugsson, A.J.M. Huxley, C.P. McCoy, J.T. Rademacher, T.E. Rice, Signaling Recognition Events with Fluorescent Sensors and Switches, Chemical Reviews, 97 (1997) 1515-1566.
[9] X. Qian, Y. Xiao, Y. Xu, X. Guo, J. Qian, W. Zhu, "Alive" dyes as fluorescent sensors: fluorophore, mechanism, receptor and images in living cells, Chemical Communications, 46 (2010) 6418-6436.
[10] F. Wang, J.H. Moon, R. Nandhakumar, B. Kang, D. Kim, K.M. Kim, J.Y. Lee, J. Yoon, Zn^{2+}-induced conformational changes in a binaphthyl-pyrene derivative monitored by using fluorescence and CD spectroscopy, Chemical Communications, 49 (2013) 7228-7230.
[11] L. Fabbrizzi, A. Poggi, Sensors and switches from supramolecular chemistry, Chemical Society Reviews, 24 (1995) 197-202.
[12] L. Prodi, F. Bolletta, M. Montalti, N. Zaccheroni, Luminescent chemosensors for transition metal ions, Coordination Chemistry Reviews, 205 (2000) 59-83.
[13] B. Valeur, I. Leray, Design principles of fluorescent molecular sensors for cation recognition, Coordination Chemistry Reviews, 205 (2000) 3-40.
[14] J.M. Berg, Y. Shi, The Galvanization of Biology: A Growing Appreciation for the Roles of Zinc, Science, 271 (1996) 1081-1085.
[15] A.I. Bush, W.H. Pettingell, G. Multhaup, M. d Paradis, J.P. Vonsattel, J.F. Gusella, K. Beyreuther, C.L. Masters, R.E. Tanzi, Rapid induction of Alzheimer A beta amyloid formation by zinc, Science, 265 (1994) 1464-1467.
[16] Z. Dai, X. Xu, J.W. Canary, Stereochemical control of Zn(II)/Cu(II) selectivity in piperidine tripod ligands, Chemical Communications, (2002) 1414-1415.
[17] J.Y. Koh, S.W. Suh, B.J. Gwag, Y.Y. He, C.Y. Hsu, D.W. Choi, The Role of Zinc in Selective Neuronal Death After Transient Global Cerebral Ischemia, Science, 272 (1996) 1013-1016.
[18] J. Lai, A. Moxey, G. Nowak, K. Vashum, K. Bailey, M. McEvoy, The efficacy of zinc supplementation in depression: Systematic review of randomised controlled trials, Journal of Affective Disorders, 136 e31-e39.
[19] J.H. Weiss, S.L. Sensi, J.Y. Koh, Zn^{2+}: A novel ionic mediator of neural injury in brain disease, Trends in Pharmacological Sciences, 21 (2000) 395-401.
[20] A.S. Prasad, Zinc deficiency, BMJ, 326 (2003) 409-410.
[21] A.S. Prasad, B. Bao, F.W.J. Beck, F.H. Sarkar, Zinc activates NF-κB in HUT-78 cells, Journal of Laboratory and Clinical Medicine, 138 (2001) 250-256.
[22] V. Bhalla, H. Arora, A. Dhir, M. Kumar, A triphenylene based zinc ensemble as an oxidation inhibitor, Chemical Communications, 48 (2012) 4722-4724.

[23] E. Hao, T. Meng, M. Zhang, W. Pang, Y. Zhou, L. Jiao, Solvent Dependent Fluorescent Properties of a 1,2,3-Triazole Linked 8-Hydroxyquinoline Chemosensor: Tunable Detection from Zinc(II) to Iron(III) in the CH_3CN/H_2O System, The Journal of Physical Chemistry A, 115 (2011) 8234-8241.
[24] X. Meng, S. Wang, Y. Li, M. Zhu, Q. Guo, 6-Substituted quinoline-based ratiometric two-photon fluorescent probes for biological Zn^{2+} detection, Chemical Communications, 48 (2012) 4196-4198.
[25] Y. Mikata, K. Kawata, S. Iwatsuki, H. Konno, Zinc-Specific Fluorescent Response of Tris(isoquinolylmethyl)amines (isoTQAs), Inorganic Chemistry, 51 (2012) 1859-1865.
[26] I. Ravikumar, P. Ghosh, Zinc(II) and PPi Selective Fluorescence OFF–ON–OFF Functionality of a Chemosensor in Physiological Conditions, Inorganic Chemistry, 50 (2011) 4229-4231.
[27] F. Sun, G. Zhang, D. Zhang, L. Xue, H. Jiang, Aqueous Fluorescence Turn-on Sensor for Zn^{2+} with a Tetraphenylethylene Compound, Organic Letters, 13 (2011) 6378-6381.
[28] Y. Zhou, Z.X. Li, S.Q. Zang, Y.Y. Zhu, H.Y. Zhang, H.W. Hou, T.C.W. Mak, A Novel Sensitive Turn-on Fluorescent Zn^{2+} Chemosensor Based on an Easy To Prepare C_3-Symmetric Schiff-Base Derivative in 100% Aqueous Solution, Organic Letters, 14 (2012) 1214-1217.
[29] D. Buccella, J.A. Horowitz, S.J. Lippard, Understanding Zinc Quantification with Existing and Advanced Ditopic Fluorescent Zinpyr Sensors, Journal of the American Chemical Society, 133 (2011) 4101-4114.
[30] L. Jiang, L. Wang, M. Guo, G. Yin, R. Y. Wang, Fluorescence turn-on of easily prepared fluorescein derivatives by zinc cation in water and living cells, Sensors and Actuators B: Chemical, 156 (2011) 825-831.
[31] K. Jobe, C.H. Brennan, M. Motevalli, S.M. Goldup, M. Watkinson, Modular 'click' sensors for zinc and their application in vivo, Chemical Communications, 47 (2011) 6036-6038.
[32] G. Kang, H. Son, J.M. Lim, H.-S. Kweon, I.S. Lee, D. Kang, J.H. Jung, Functionalized Fe3O4 Nanoparticles for Detecting Zinc Ions in Living Cells and Their Cytotoxicity, Chemistry – A European Journal, 18 (2012) 5843-5847.
[33] Y. Mikata, A. Yamashita, K. Kawata, H. Konno, S. Itami, K. Yasuda, S. Tamotsu, Methoxyquinoline-diethylenetriamine conjugate as a fluorescent zinc sensor, Dalton Transactions, 40 (2011) 4976-4981.
[34] K. Velmurugan, J. Prabhu, L. Tang, T. Chidambaram, M. Noel, S. Radhakrishnan, R. Nandhakumar, A simple chalcone-based fluorescent chemosensor for the detection and removal of Fe^{3+} ions using a membrane separation method, Analytical Methods, 6 (2014) 2883-2888.
[35] P. Du, S.J. Lippard, A Highly Selective Turn-On Colorimetric, Red Fluorescent Sensor for Detecting Mobile Zinc in Living Cells, Inorganic Chemistry, 49 (2010) 10753-10755.
[36] H.Y. Li, S. Gao, Z. Xi, A colorimetric and “turn-on” fluorescent chemosensor for Zn(II) based on coumarin Shiff-base derivative, Inorganic Chemistry Communications, 12 (2009) 300-303.

[37] S. Maruyama, K. Kikuchi, T. Hirano, Y. Urano, T. Nagano, A Novel, Cell-Permeable, Fluorescent Probe for Ratiometric Imaging of Zinc Ion, Journal of the American Chemical Society, 124 (2002) 10650-10651.
[38] S.H. Mashraqui, R. Betkar, S. Ghorpade, S. Tripathi, S. Britto, A new internal charge transfer probe for the highly selective detection of Zn(II) by means of dual colorimetric and fluorescent turn-on responses, Sensors and Actuators B: Chemical, 174 (2012) 299-305.
[39] K. Velmurugan, A. Raman, D. Don, L. Tang, S. Easwaramoorthi, R. Nandhakumar, Quinoline benzimidazole-conjugate for the highly selective detection of Zn(II) by dual colorimetric and fluorescent turn-on responses, RSC Advances, 5 (2015) 44463-44469.
[40] F.B. Miguel, J.A. Dantas, S. Amorim, G.F.S. Andrade, L.A.S. Costa, M.R.C. Couri, Synthesis, spectroscopic and computational characterization of the tautomerism of pyrazoline derivatives from chalcones, Spectrochimica Acta Part A: Molecular and Biomolecular Spectroscopy, 152 (2016) 318-326.
[41] C. Lee, W. Yang, R.G. Parr, Development of the Colle-Salvetti correlation-energy formula into a functional of the electron density, Physical Review B, 37 (1988) 785-789.
[42] W. R. Wadt, P.J. Hay, Ab initio effective core potentials for molecular calculations. Potentials for main group elements Na to Bi, The Journal of Chemical Physics, 82 (1985) 284-298.
[43] P. J. Hay, W.R. Wadt, Ab initio effective core potentials for molecular calculations. Potentials for the transition metal atoms Sc to Hg, The Journal of Chemical Physics, 82 (1985) 270-283.
[44] P .J. Hay, W.R. Wadt, Ab initio effective core potentials for molecular calculations. Potentials for K to Au including the outermost core orbitals, The Journal of Chemical Physics, 82 (1985) 299-310.
[45] J. Tomasi, B. Mennucci, R. Cammi, Quantum Mechanical Continuum Solvation Models, Chemical Reviews, 105 (2005) 2999-3094.
[46] M.J. Frisch, G.W. Trucks, H.B. Schlegel, G.E. Scuseria, M.A. Robb, J.R. Cheeseman, G. Scalmani, V. Barone, B. Mennucci, G.A. Petersson, H. Nakatsuji, M. Caricato, X. Li, H.P. Hratchian, A.F. Izmaylov, J. Bloino, G. Zheng, J.L. Sonnenberg, M. Hada, M. Ehara, K. Toyota, R. Fukuda, J. Hasegawa, M. Ishida, T. Nakajima, Y. Honda, O. Kitao, H. Nakai, T. Vreven, J.A. Montgomery Jr., J.E. Peralta, F. Ogliaro, M.J. Bearpark, J. Heyd, E.N. Brothers, K.N. Kudin, V.N. Staroverov, R. Kobayashi, J. Normand, K. Raghavachari, A.P. Rendell, J.C. Burant, S.S. Iyengar, J. Tomasi, M. Cossi, N. Rega, N.J. Millam, M. Klene, J.E. Knox, J.B. Cross, V. Bakken, C. Adamo, J. Jaramillo, R. Gomperts, R.E. Stratmann, O. Yazyev, A.J. Austin, R. Cammi, C. Pomelli, J.W. Ochterski, R.L. Martin, K. Morokuma, V.G. Zakrzewski, G.A. Voth, P. Salvador, J.J. Dannenberg, S. Dapprich, A.D. Daniels, Ö. Farkas, J.B. Foresman, J.V. Ortiz, J. Cioslowski, D.J. Fox, Gaussian 09, in, Gaussian, Inc., Wallingford, CT, USA, 2009.

[47] H. Ghaffari, M. Venkataramana, B. Jalali Ghassam, S. Chandra Nayaka, A. Nataraju, N.P. Geetha, H.S. Prakash, Rosmarinic acid mediated neuroprotective effects against H_2O_2-induced neuronal cell damage in N2A cells, Life Sciences, 113 (2014) 7-13.
[48] M. M. Ali, K. C. Tasneem, P.K. Rajanna, P. Sai, An Efficient and Facile Synthesis of 2-Chloro-3-formyl Quinolines from Acetanilides in Micellar Media by Vilsmeier-Haack Cyclisation, Synlett, 2001 (2001) 0251-0253.
[49] S. Santhoshkumar, K. Velmurugan, J. Prabhu, G. Radhakrishnan, R. Nandhakumar, A naphthalene derived Schiff base as a selective fluorescent probe for Fe_{2+}, Inorganica Chimica Acta, 439 (2016) 1-7.
[50] K. Velmurugan, R. Nandhakumar, Binol based "turn on" fluorescent chemosensor for mercury ion, Journal of Luminescence, 162 (2015) 8-13.
[51] H. Irving, H. Freiser, T. West, IUPAC compendium of analytical nomenclature, definitive rules, in, Pergamon Press, Oxford, 1981.
[52] W.H. Melhuish, Quantum efficiencies of fluorescence of organic substances: Effect of solvent and concentration of the fluorescent solute1, The Journal of Physical Chemistry, 65 (1961) 229-235.
[53] L. Tang, N. Wang, Q. Zhang, J. Guo, R. Nandhakumar, A new benzimidazole-based quinazoline derivative for highly selective sequential recognition of Cu^{2+} and CN^{-}, Tetrahedron Letters, 54 (2013) 536-540.
[54] J. Prabhu, K. Velmurugan, R. Nandhakumar, Development of fluorescent lead II sensor based on an anthracene derived chalcone, Spectrochimica Acta Part A: Molecular and Biomolecular Spectroscopy, 144 (2015) 23-28.
[55] F. Wang, R. Nandhakumar, J.H. Moon, K.M. Kim, J.Y. Lee, J. Yoon, Ratiometric Fluorescent Chemosensor for Silver Ion at Physiological pH, Inorganic Chemistry, 50 (2011) 2240-2245.
[56] K. Velmurugan, S. Suresh, S. Santhoshkumar, M. Saranya, R. Nandhakumar, A simple Chalcone-based ratiometric chemosensor for silver ion, Luminescence, 31 (2016) 722-727.
[57] V. Kalfakakou, T.J. Simons, Anionic mechanisms of zinc uptake across the human red cell membrane, The Journal of Physiology, 421 (1990) 485-497.
[58] D.M.T. Lorella M. T. Canzoniero, and Dennis W. Choi, Measurement of intracellular free zinc concentrations accompanying zinc-induced neuronal death, J. Neurosci, 19 (1999).
[59] C. Karunakaran, J. Jayabharathi, K. Jayamoorthy, K. Brindha Devi, Sensing rutile TiO2 through fluorescence of imidazole derivative, Sensors and Actuators B: Chemical, 168 (2012) 263-270.
[60] R. Krolicki, W. Jarzeba, M. Mostafavi, I. Lampre, Preferential Solvation of Coumarin 153The Role of Hydrogen Bonding, The Journal of Physical Chemistry A, 106 (2002) 1708-1713.
[61] T. Molotsky, D. Huppert, Site Specific Solvation Statics and Dynamics of Coumarin Dyes in Hexane−Methanol Mixture, The Journal of Physical Chemistry A, 107 (2003) 2769-2780.

[62] J. Prabhu, K. Velmurugan, R. Nandhakumar, Pb^{2+} ion induced self assembly of anthracene based chalcone with a fluorescence turn on process in aqueous media, J Anal Chem, 70 (2015) 943-948.
[63] K.V. S. Suresh, S. Santoshkumar, J. Prabhu and R. Nandhakumar, Pb^{2+} - Induced Self Assembly of a Thiophene Derived Chalcone With Enhanced Fluorescence in Aqueous Media, J Chem Applied Biochem, 1 (2014) 103.
[64] R. Satheeshkumar, R. Shankar, W. Kaminsky, S. Kalaiselvi, V.V. Padma, K.J. Rajendra Prasad, Theoretical and experimental investigations on molecular structure of 7-Chloro-9-phenyl-2,3-dihydroacridin-4(*1H*)-one with cytotoxic studies, Journal of Molecular Structure, 1109 (2016) 247-257.
[65] M. Iniya, D. Jeyanthi, K. Krishnaveni, A. Mahesh, D. Chellappa, Triazole based ratiometric fluorescent probe for Zn^{2+} and its application in bioimaging, Spectrochimica Acta Part A: Molecular and Biomolecular Spectroscopy, 120 (2014) 40-46.
[66] Y. Mikata, A. Yamashita, A. Kawamura, H. Konno, Y. Miyamoto, S. Tamotsu, Bisquinoline-based fluorescent zinc sensors, Dalton Transactions, (2009) 3800-3806.
[67] D. Maity, T. Govindaraju, Naphthaldehyde–Urea/Thiourea Conjugates as Turn-On Fluorescent Probes for Al^{3+} Based on Restricted C=N Isomerization, European Journal of Inorganic Chemistry, 2011 (2011) 5479-5485.
[68] K. Velmurugan, A. Raman, S. Easwaramoorthi, R. Nandhakumar, Pyrene pyridine-conjugate as Ag selective fluorescent chemosensor, RSC Advances, 4 (2014) 35284-35289.

[69] C. Yuan, S. Li, Y. Wu, L. Lu, M. Zhu, Zn(II)-selective and sensitive fluorescent chemosensor based on steric constrains and inhibition of ESIPT, Sens. Actuators, B, 242 (2017) 1035–1042.
[70] M. Kumar, A. Kumar, M.K. Singh, S.K. Sahu, R.P. John, A novel benzidine based Schiff base “turn-on” fluorescent chemosensor for selective recognition of Zn^{2+}, Sens. Actuators, B, 241 (2017) 1218–1223.

[71] Y. Li, K. Li, J. He, A “turn-on” fluorescent chemosensor for the detection of Zn(II) in aqueous solution at neutral pH and its application in live cells imaging, Talanta, 153 (2016) 381–385.

[72] Y. Jin, S. Wang, Y. Zhang, B. Song, Highly selective fluorescent chemosensor based on benzothiazole for detection of Zn^{2+}, Sens. Actuators, B, 225 (2016) 167–173.

[73] D. Sarkar, A. Pramanik, S. Jana, P. Karmakar, T.K. Mondal, Quinoline based reversible fluorescent ‘turn-on’ chemosensor for the selective detection of Zn^{2+}: Application in living cell imaging and as INHIBIT logic gate, Sens. Actuators, B, 209 (2015) 138–146.

[74] P. Wang, J. Wu, P. Su, C. Shan, P. Zhou, Y. Ge, D. Liu, W. Liu, Y. Tang, A novel fluorescent chemosensor based on tetra-peptides for detecting zinc ions in aqueous solutions and live cells, J. Mater. Chem. B, 4 (2016) 4526-4533.

[75] K. Tayade, B. Bondhopadhyay, K. Keshav, S.K. Sahoo, A. Basu, J. Singh, N. Singh, D.T. Nehete, Anil Kuwar, A novel Zinc(II) and Hydrogen sulphate selective fluorescent "turn-on" chemosensor based on isonicotiamide: INHIBIT type's logic gate and application in cancer cell imaging, Analyst, 141 (2016) 1814-1821.

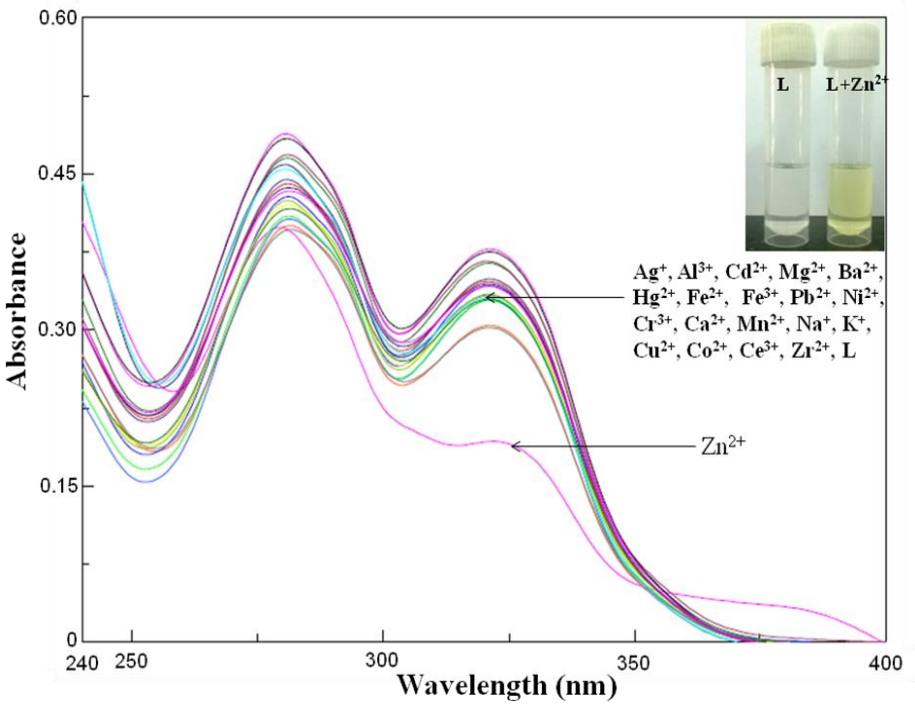

Fig. 1. UV-Vis absorption changes of **L** (2×10^{-6} M) in the presence of different metal ions (50 equiv.) in EtOH-H_2O (1:1 v/v, HEPES= 50 mM, pH= 7.2) solution.

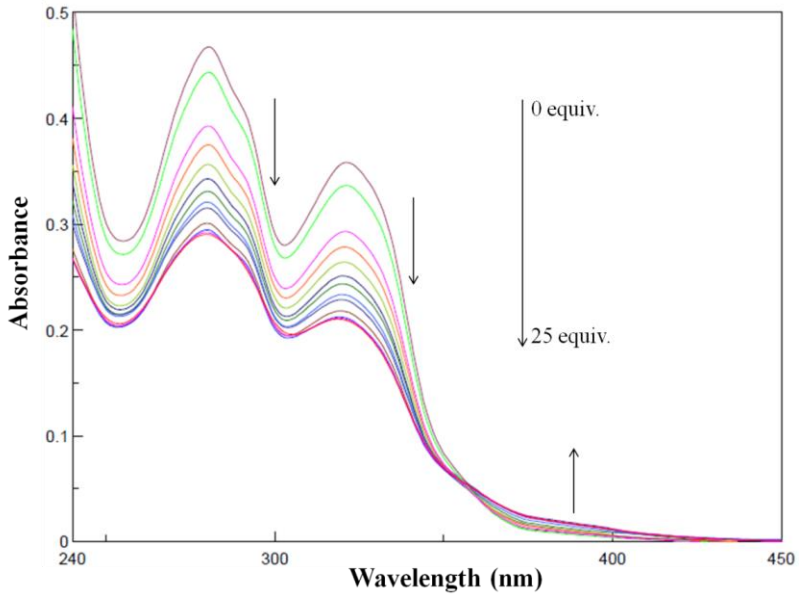

Fig. 2. Changes in absorption intensity of **L** (2×10^{-6} M) solution (EtOH-H_2O, 1:1 v/v, HEPES= 50 mM, pH= 7.2) upon addition of different amount of Zn^{2+} (0-25 equiv.).

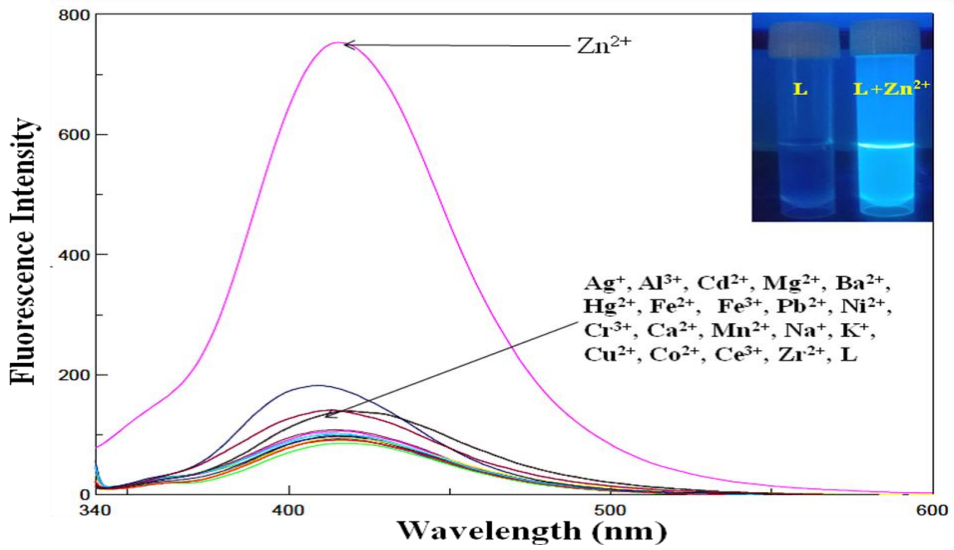

Fig. 3. Fluoresence changes of **L** (2×10^{-6} M) solution (EtOH/H_2O, 1:1 v/v, HEPES= 50 mM, pH= 7.2) in the presence of various metal ions (50 equiv.).

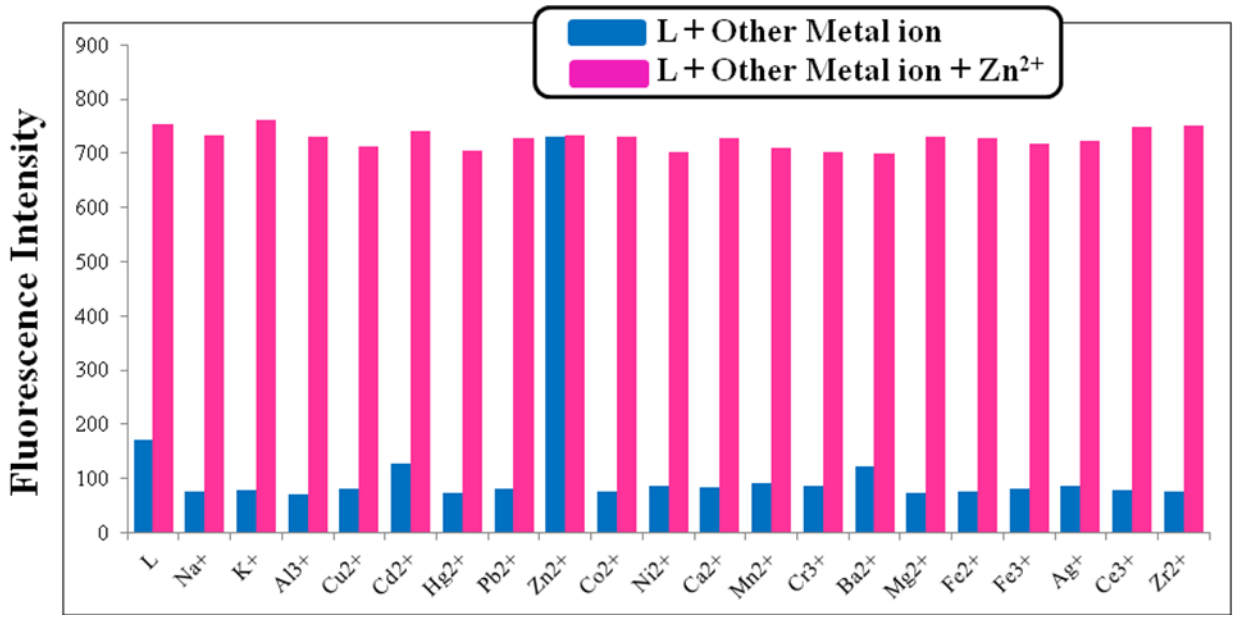

Fig. 4. Metal ions competition analysis of **L** ($2X10^{-6}$ M) in $EtOH/H_2O$, 1: 1 v/v, HEPES = 50 mM, pH=7.2. The blue bars represent fluorescence emission of **L** and 50 equiv. of other metal ions. The pink bars represent fluorescence changes that occur upon addition of 50 equiv. of other metal ions to solution containing **L** and Zn^{2+} (50 equiv.).

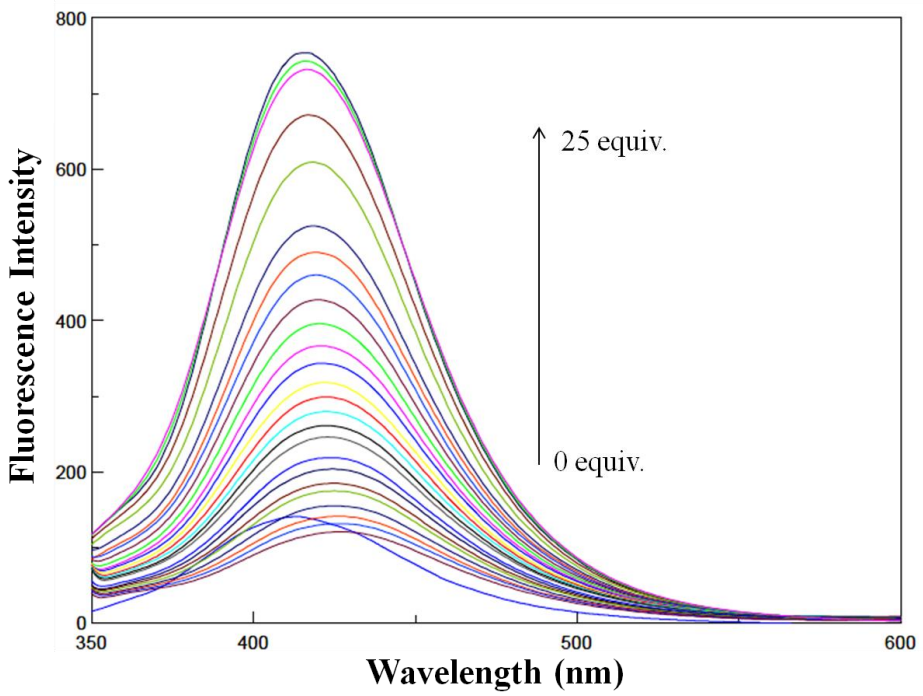

Fig. 5. Fluorescence spectra of **L** obtained upon addition of Zn^{2+} (0-25 equiv.)in EtOH/H_2O mixture (1:1, v/v) using HEPES buffer at pH=7.2.

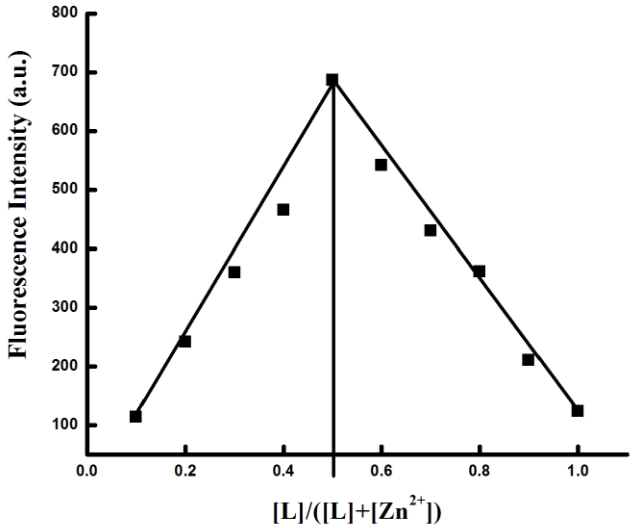

Fig. 6. Job's plot for **L** with Zn^{2+} ions in EtOH/H_2O (1:1 (v/v), HEPES = 50 mM, pH= 7.2) solution.

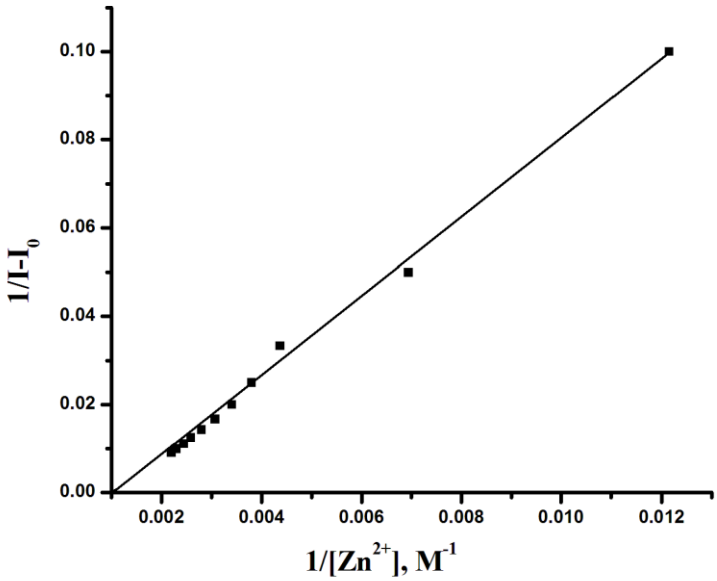

Fig. 7. Benesi- Hildebrand plot of **L**-Zn^{2+} complex (1:1) stoichiometry.

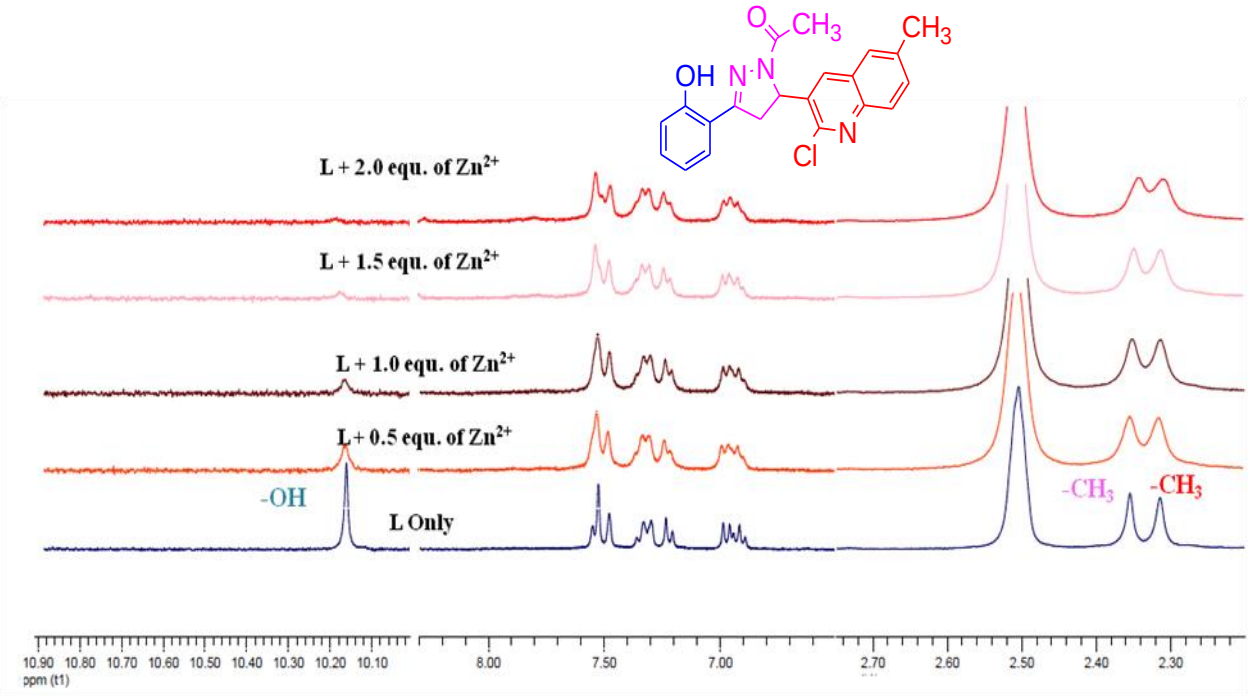

Fig. 8. Partial ^{1}H- NMR spectra of **L** and **L**- Zn^{2+}.

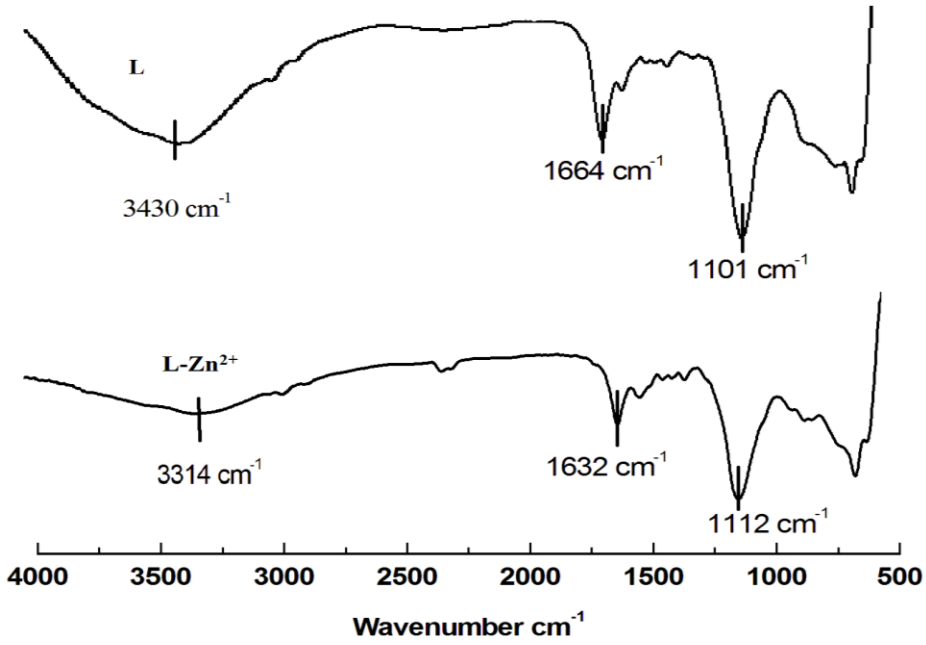

Fig. 9. FT-IR spectra of **L** and **L**-Zn^{2+}.

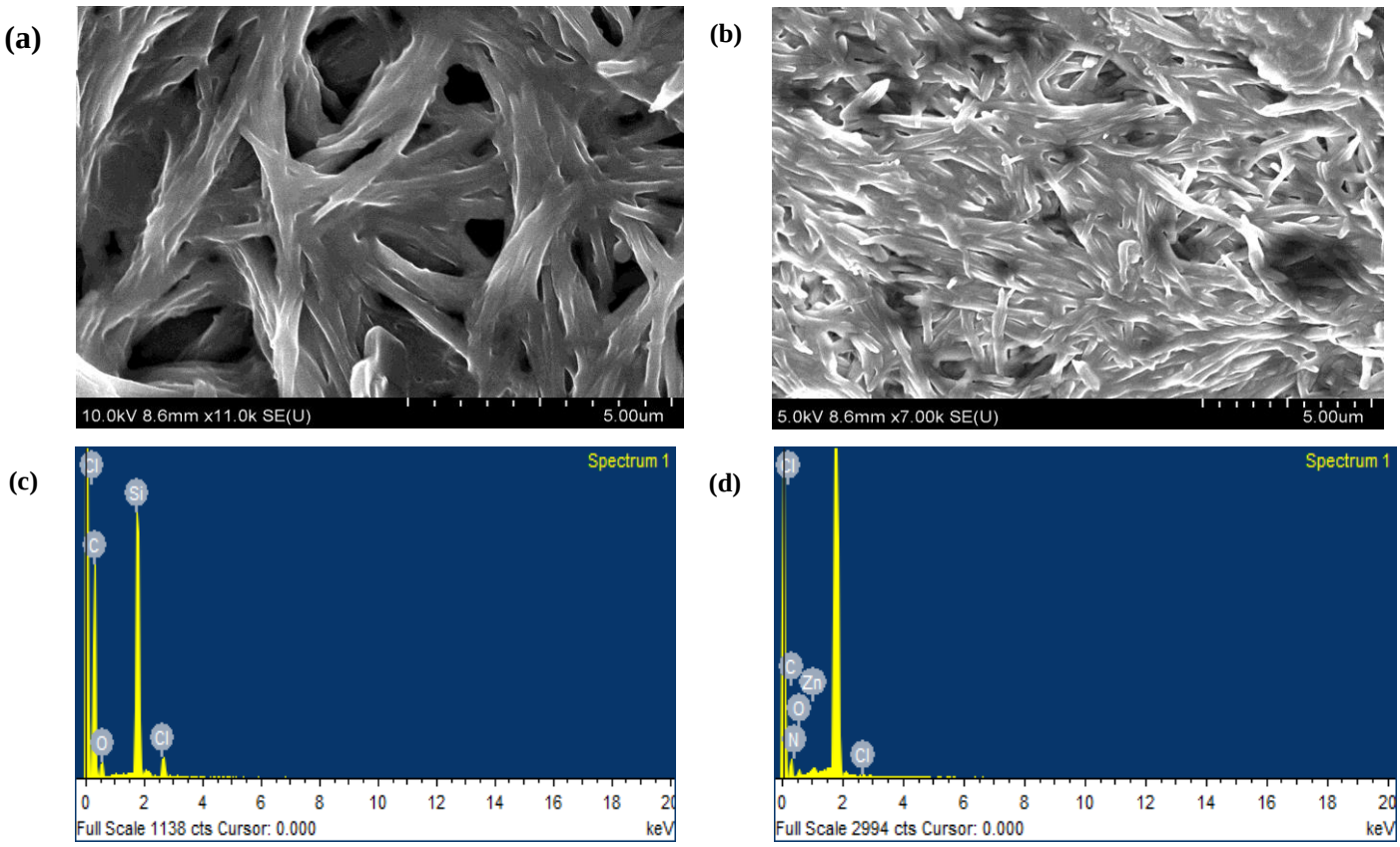

Fig. 10. SEM images of (a) Probe **L** and (b) **L**+ $Zn(NO_3)_2$. EDX analysis of (c) Probe **L** and (d) **L**+ $Zn(NO_3)_2$

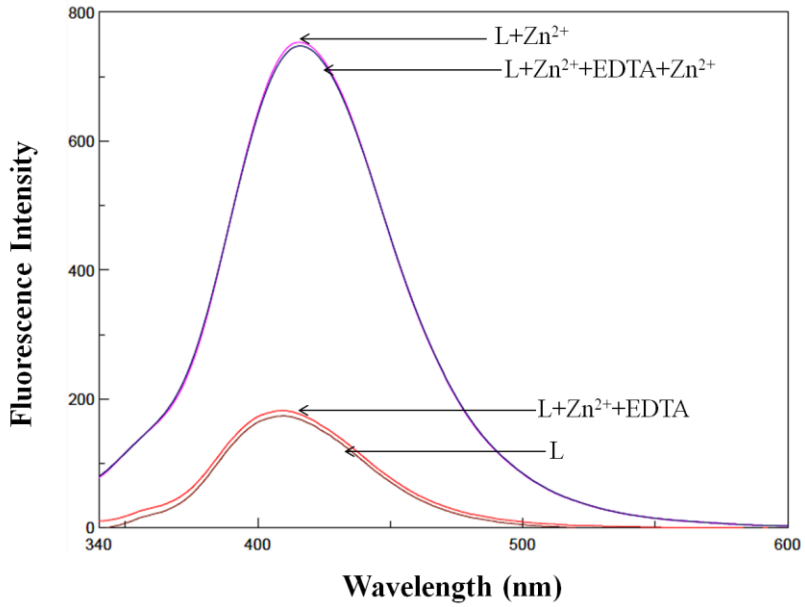

Fig. 11. Fluoresence spectra of **L** (2×10^{-6} M) solution ($EtOH/H_2O$, 1:1 v/v, HEPES= 50 mM, pH= 7.2) in the presence of Zn^{2+} (50 equiv.) and EDTA (50 equiv.).

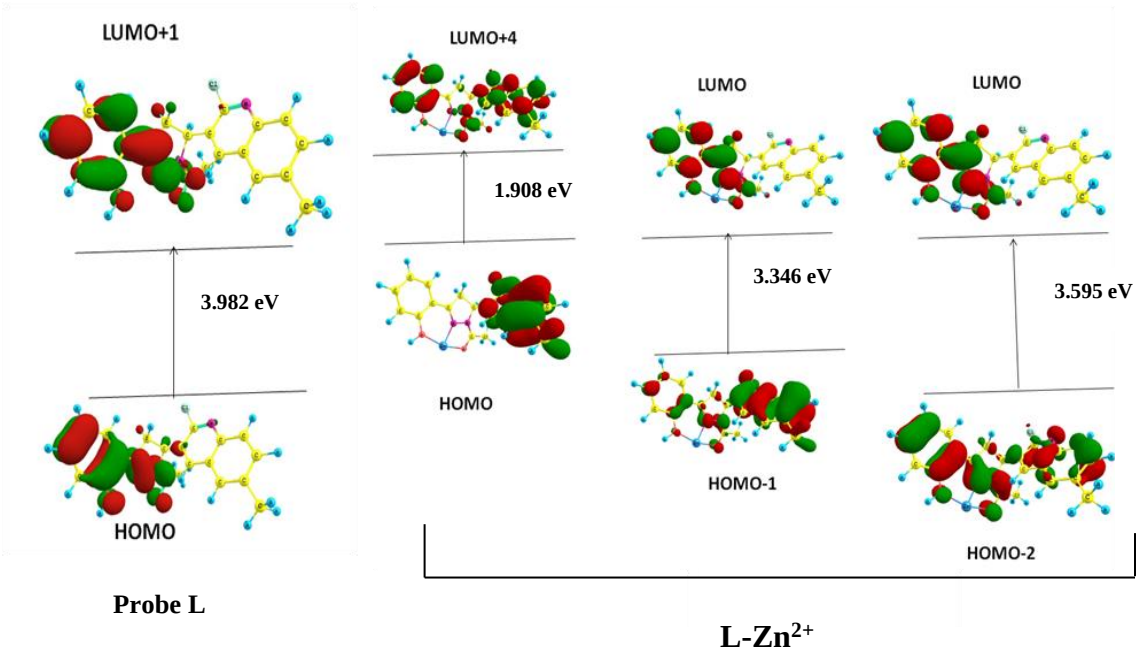

Fig. 12. Frontier molecular orbitals of **L** and **L**-Zn^{2+} obtained from the DFT calculations using Guassian 09 program.

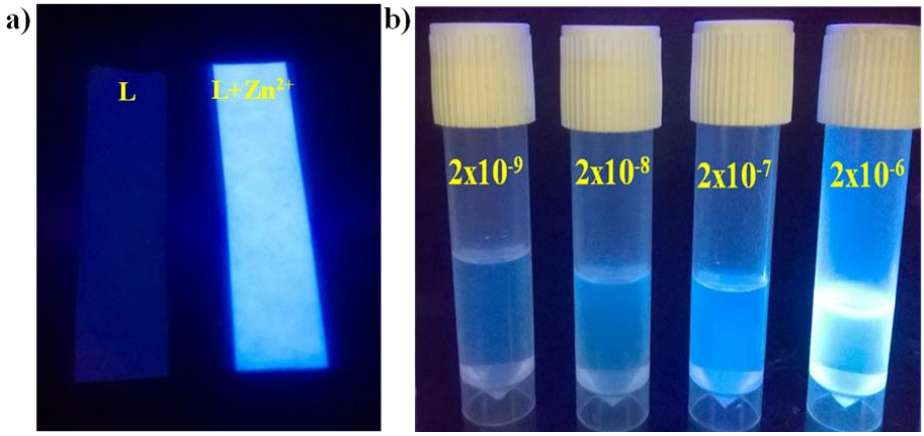

Fig. 13. (a) Visible colour change in test strips after the addition of Zn^{2+} (2 μM) under UV light irradiation. (b) Sample tubes containing probe **L** (2 μM) solution with different concentrations of the Zn^{2+} ions under UV light irradiation.

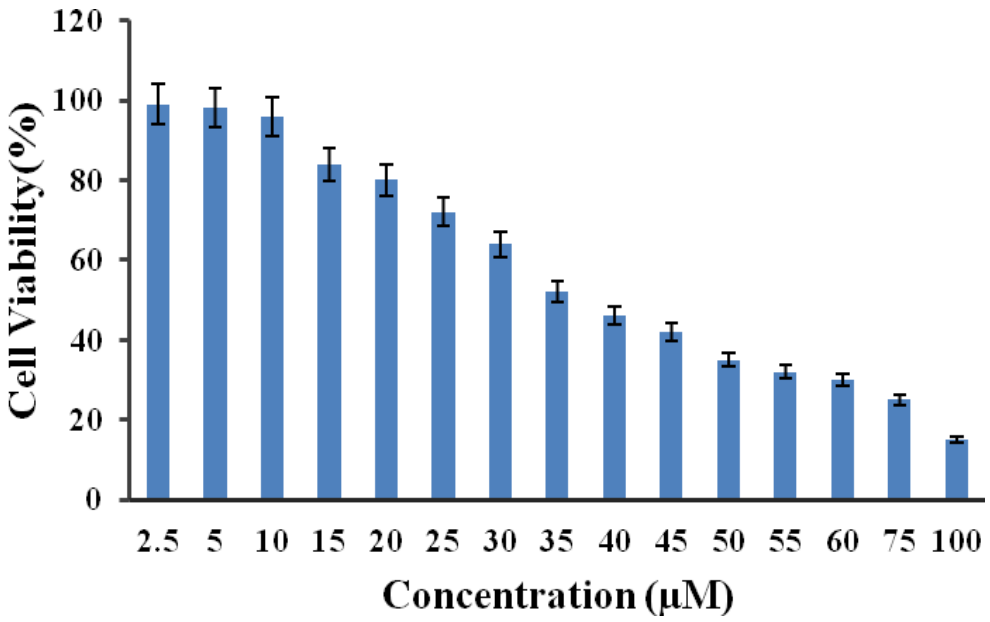

Fig. 14. Cell viability graph of probe **L** using N2A cells by MTT assay.

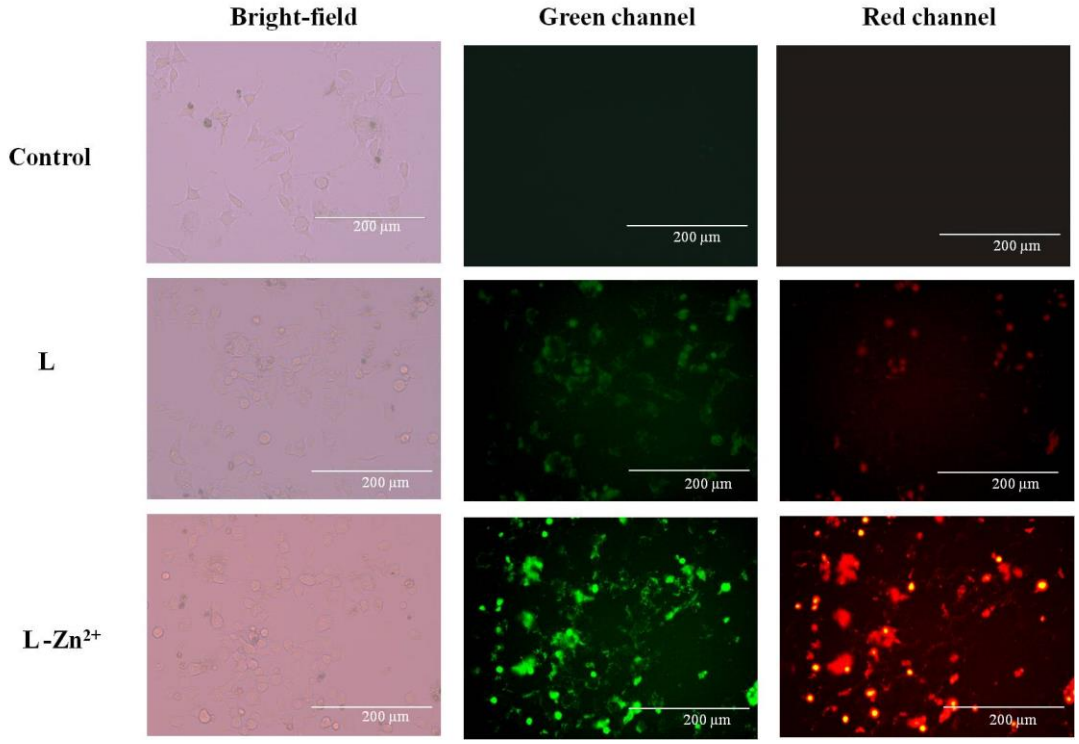

Fig. 15. Fluorescence images of N2A cells. Bright field images of control (absence of **L** and Zn^{2+}), **L** (10 µM) and **L**-Zn^{2+} (10 µM) (Left). Fluorescence microscopic images of control, **L** and **L**-Zn^{2+} in green channel (centre) and in red channel (right).

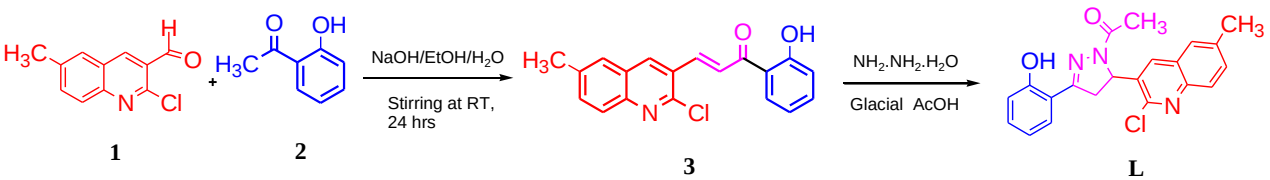

1 **2** **3** **L**

Scheme 1. Synthesis of probe **L**.

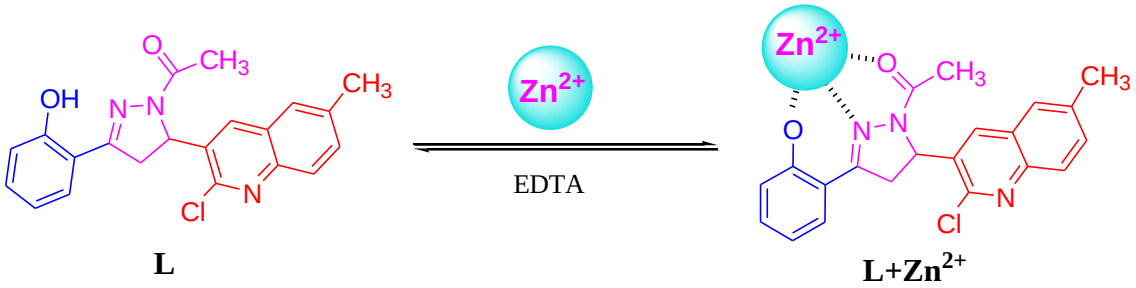

L **L+Zn^{2+}**

Scheme. 2. Proposed binding mode of **L** with Zn^{2+}.

Table 1: The comparison of detection limits of probe **L** with reported chemosensors available in the literature.

References	Ions	Detection limit
Our Probe L	**Zn^{2+}**	**2.9×10^{-9} M**
[69]	Zn^{2+}	0.69 μM
[70]	Zn^{2+}	8.6×10^{-9} M
[71]	Zn^{2+}	70 nmol L^{-1}
[72]	Zn^{2+}	7.5×10^{-7} $molL^{-1}$
[73]	Zn^{2+}	5.0×10^{-9} M
[74]	Zn^{2+}	32 nM
[75]	Zn^{2+}	3.81 nM